ACS ORGANIC & INORGANIC Au
AN OPEN ACCESS JOURNAL OF THE AMERICAN CHEMICAL SOCIETY

pubs.acs.org/orginorgau
Review

Applications of Antimony in Catalysis

Lewen Wu, Choon-Hong Tan,* and Xinyi Ye*

Cite This: ACS Org. Inorg. Au 2025, 5, 13−25
Read Online
ACCESS | Metrics & More | Article Recommendations

ABSTRACT: Antimony is a fifth-period element in the nitrogen family, a silver-white metalloid with weak conductivity and thermal conductivity. It is stable at room temperature and does not react easily with oxygen and water in the air. Natural minerals are found in the form of sulfides. Current research and applications are mostly concentrated on material modification, utilizing the properties of antimony in traditional chemical industries, helping alloys improve their flame retardancy, stability, increasing semiconductor performance, etc. For example, to enhance the electronic conductivity, after coating or embedding antimony or its derivatives in thin layers in photonic nanomaterials, the performance of the original material in photoelectrochemical catalysis can be effectively increased, thereby expanding the efficiency of oxidation−reduction reactions accounting for the degradation of organic matter in wastewater. However, the catalytic reaction between the derivatives of antimony and organic compounds beside the material is less studied, and the mechanism of the studies in organic synthesis is relatively unclear. The reported organic synthesis related to antimony is mainly in the form of Lewis acid catalysts or dual-metal catalytic systems combined with other metals. This Review will focus on the application of antimony in photocatalysis, electrocatalysis, and other organic syntheses in the past 10 years.

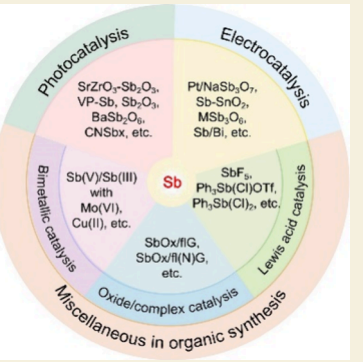

KEYWORDS: *antimony, photocatalysis, electrocatalysis, water splitting, organic synthesis, Lewis acid catalyst, dual catalysis, bimetallic catalysis, antimony oxide, antimony complex*

1. INTRODUCTION

The term "pnigogen" was originally coined by van Arkel in the Canadian Journal of Chemistry in 1961 to describe the elemental forms of group 15 elements. By around 1990, this term evolved into "pnicogen" or "pnictogen".[1] Until the revised inorganic nomenclature was proposed in 2005, IUPAC referred to group 15 elements and their compounds as "phosphorus elements" and "phosphorus compounds", respectively.[2]

Lately, there has been growing desire to employ group 15 reagents as catalysts.[3] Antimony (Sb), which belongs to group 15, is commonly found in trivalent Sb(III) and pentavalent Sb(V) forms.[4] Group 15 elements, such as phosphorus, arsenic, antimony, and bismuth, can serve as donor atoms. The interaction known as the antimonic bond or nitrogen group element bond (PnB) involves a σ-hole interaction between an electron-deficient area on the surface and a nucleophile (electron-rich acceptor).[5,6] This type of interaction enables reactivity that is different from that observed in traditional Lewis acid catalysis.[7]

Antimonides, characterized as strong Lewis acids, have found applications as catalysts or reagents in various organic reactions. Experimental evidence indicates that $SbCl_5$ exhibits higher chloride ion affinity than BCl_3, indicating its superior Lewis acidity.[8] However, the corrosive nature of antimony halides, such as $SbCl_5$, has led to the development of modified antimony derivatives with substituents. While these derivatives may be less acidic than the corresponding antimony halides, they exhibit excellent stability to water and oxygen, coupled with high Lewis acidity and relative stability.[9] Examples include antimony triphenyl (V) pentafluorobenzenesulfonate and perfluorinated octanesulfonate, both showcasing exceptional hydrolysis resistance and thermal stability.[10]

Research has demonstrated that pure antimony oxide exhibits relative inertness and significantly influences catalyst activity.[11] Furthermore, antimony plays a crucial role in the structural stability and functionality of numerous crystal structures reported in the literature.[12]

Antimony and its derivatives can be used as catalysts; meanwhile, they also have a wide range of other applications, such as antimony selenide, which is common in solar cells, photodetectors, battery electrodes, and memory devices.[13] Two-dimensional antimonene quantum dots with high photothermal conversion efficiency have been used as novel near-infrared photothermal agents for effective cancer treatment in the biomedical field.[14,15] Antimony chloride can be used for information anticounterfeiting, encryption decryption, and

Received: September 20, 2024
Revised: October 28, 2024
Accepted: October 28, 2024
Published: November 6, 2024

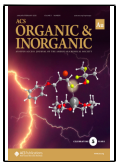

https://doi.org/10.1021/acsorginorgau.4c00072
ACS Org. Inorg. Au 2025, 5, 13−25

logic gate construction, having potential application value in the fields of anticounterfeiting and encryption.[16]

In this Review, we explore the historical aspects of antimony and provide an overview of the research progress concerning constructed antimonides and their derivatives as catalysts (Figure 1), spanning the period from 2014 to 2024.

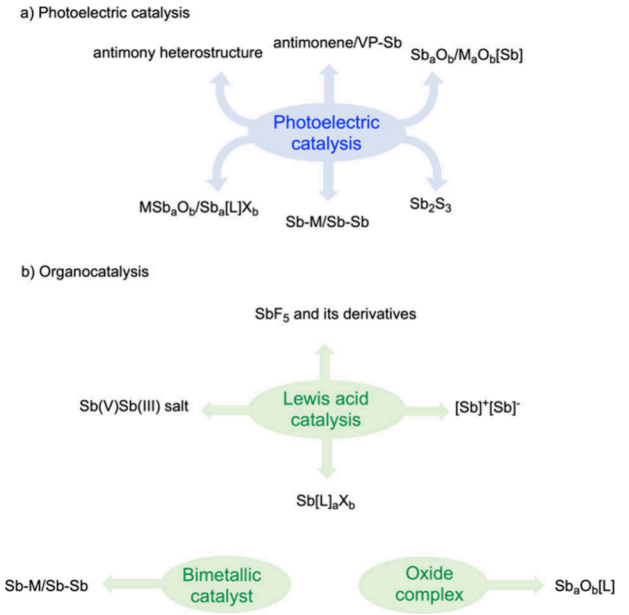

Figure 1. Antimony derivatives.

2. APPLICATIONS

2.1. Applications of Antimony in Photocatalysis

In recent times, there has been increasing focus on the role of photocatalysis in advancing environmentally sustainable synthesis techniques.[17] Photocatalysis involves the utilization of metal complexes activated by visible light as catalysts in organic synthesis.[18] The application of metal-based photocatalysts in organic chemistry was validated in the late 1970s, and significant advancements have been made in the past 15 years, leading to the construction of synthesis methods for numerous molecules and products.[19] Common visible-light catalysts include metal oxides like TiO_2,[20] and polypyridine complexes of ruthenium and iridium such as $Ru(bpy)_3^{2+}$ and [Ir(tpy)(R-ppy)Cl] (Figure 2).[21,22]

Despite these progressions, issues like the limited spectral response range of TiO_2 and the energy requirements for light or heat have constrained the photocatalytic effectiveness and applicability of certain catalysts.[23−25] In recent years, antimony-based photocatalysts have garnered growing attention for their superior photocatalytic activity compared to TiO_2.[26]

For example, Guo and colleagues developed a photocatalyst by doping Sb into TiO_2 and used a fluorescent probe, terephthalic acid, to assess its effectiveness. The incorporation of Sb into TiO_2 lowered the energy barrier for bond formation, facilitating easier radical initiation compared to pure TiO_2. This modification extended the absorption spectrum, from UV to visible light, and strengthened the photocatalytic performance.[27] Zhou and colleagues used the scraper method to fabricate a mesoporous composite film of titanium dioxide (TiO_2) and antimony-doped tin oxide (ATO) on a titanium plate matrix. Under ultraviolet light, methylene blue was selected to probe the degradation. It was found that the coating ratio had a significant effect on the testing of the photoelectric effect. In the experiments, different proportions of ATO nanoparticles mixed with TiO_2 were used to prepare composite films, which were tested for their photocatalytic properties. The results showed that the photocatalytic performance of the composite films significantly improved with the increase of the ATO ratio. When the proportion of ATO was 10%, the degradation rate of the composite film reached 94%, while the degradation rate of the pure TiO_2 film was only 41.2%. This indicates that the addition of ATO nanoparticles can significantly improve the photocatalytic activity of the composite films. It was also found that the charge transport and transfer properties of the composite films improved as the ratio of ATO was increased. The charge transport resistance (R_b) and interfacial charge transfer resistance (R_i) of the composite films decrease with increasing ATO ratio, indicating that the introduction of ATO nanoparticles contributes to the improvement of charge transport and transfer rates (Figure 3).[28]

In 2017, Nakata and his team developed a Rh−Sb codoped $SrTiO_3$ photocatalyst (STO:Rh,Sb). The inclusion of antimonate significantly hindered the formation of the Rh^{4+} composite center in STO. Additionally, the photocatalytic degradation of acetaldehyde demonstrated that the photo-

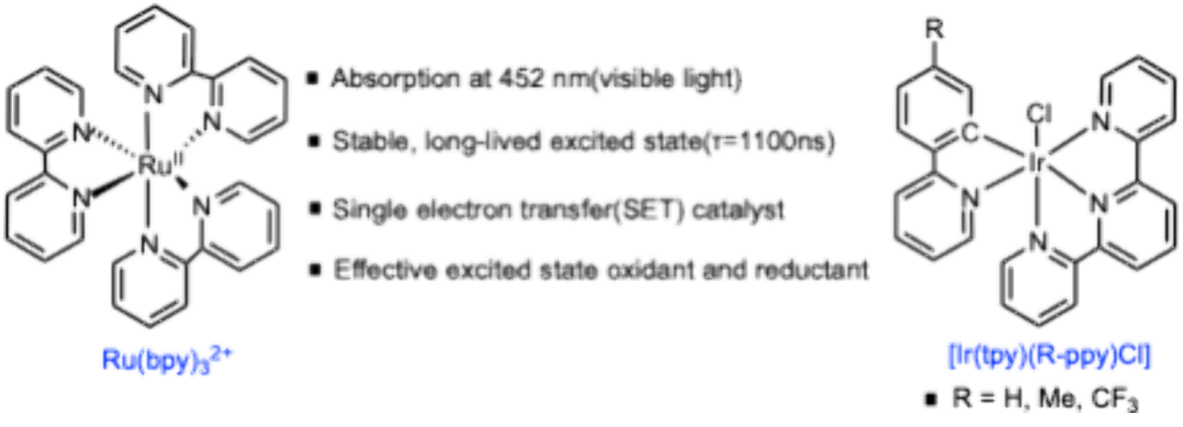

Figure 2. Ruthenium polypyridyl complexes and iridium polypyridyl complexes: versatile visible-light photocatalysts.

https://doi.org/10.1021/acsorginorgau.4c00072
ACS Org. Inorg. Au 2025, 5, 13−25

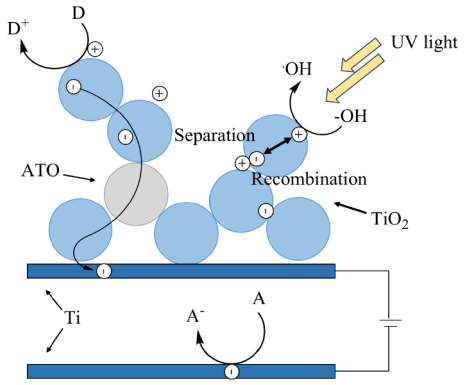

Figure 3. Scheme of the photoelectrocatalytic process with and without ATO.

catalytic efficiency of ground STO:Rh,Sb was superior to that of ground STO without antimony doping.[29]

Chen and co-workers conducted a photocatalytic breakdown experiment of rhodamine B (RhB) and discovered that Sb-doped $(BiO)_2CO_3$ nanosheets exhibited a notable increase in photocatalytic activity compared to pure $(BiO)_2CO_3$ nanosheets. This enhanced activity was credited to a larger surface area and a faster electron transfer rate.[30] Li and colleagues found that in the process of the photocatalytic breakdown of RhB, the accumulating concentration of •OH radicals was dependent on the form of $BaSb_2O_6$. The form of $BaSb_2O_6$ greatly affected the photocatalytic activity. The authors compared the marigold-flower-like $BaSb_2O_6$ (M-$BaSb_2O_6$), rose-flower-like $BaSb_2O_6$ (R-$BaSb_2O_6$), and ground samples of these two forms, demonstrating the active species in the photocatalytic process.[31]

The following year, He's group investigated how Sb(III) photooxidation occurs with various Fe(III) species and discovered that at pH 1−3 the primary oxidants for Sb(III) oxidation were •OH and $•Cl_2^-$ radicals. According to the control experiment results, the •OH radical dominated the redox process. With the accumulation of OH^-, the aqueous condition changed to be basic, and during this stage an electron transfer happened between Sb(III) and Fe(III), leading to the formation of Fe(II). The findings illustrated that the geochemical cycling of Sb(III) in aquatic systems heavily depended on various sources of Fe(III).[32]

Férid's group employed Sb-doped ZnO nanocrystals (NCs) to enhance visible light absorption of ZnO-NCs. By using RhB as probes, Sb-doped ZnO NCs promoted hydroxyl radical generation and improved the photocatalytic reaction rate.[33] Torres-Martínez's group designed a $SrZrO_3$−Sb_2O_3 heterostructure that demonstrated 30% higher activity than $SrZrO_3$ due to effective charge separation and transmission at the heterostructure interface. In application exploration, they used it to deal with water splitting and the degradation of biohazard tetracyclines.[34]

In 2018, Zamora's group created a sandwiched form of heterostructures with carbon nitride and antimonene flakes, which improved light absorption and charge separation and exhibited higher photocatalytic activity in organic pollutant degradation.[35] Mohamed and co-workers prepared silver-doped Sb_2O_3 nanocomposites to prepare aniline via the photoredeox reaction of nitrobenzene. They discovered the enhancement of photocatalytic activity due to a reduction in the band gap and the extended lifetime of electron−hole pairs.[36]

To enhance the photocatalytic activity of Sb_2O_3, Riaz and co-workers tried to combine Sb_2O_3 with poly(*o*-phenylenediamine) (POPD) to form nanocomposites through in situ oxidation polymerization. The screening results showed that Sb_2O_3 loaded with 24% POPD had higher thermal stability than pure Sb_2O_3 and also showed good photocatalytic activity.[37]

Kokabi's group studied the single-layer antimonene nanosheets and found they exhibited photocatalytic properties across the entire pH range.[38] Both armchair and zigzag directions were explored, and the armchair edges were more chemically active. The maximum number of atoms was up to 388. In the application of water splitting experiments, both morphologies of nanosheets had great potential to be promising photocatalysts.

Antimony's influence on photocatalytic properties extends beyond just improving photosensitizers; it also affects other nonphotocatalytic reagents. In 2021, Dai's group developed an ultrathin van der Waals heterostructure of antimony/graphitic carbon nitride (Sb/g-C_3N_4) to facilitate carbon dioxide reduction. The photocatalytic performance showed that this heterostructure enhanced CO_2 activation due to its increased specific surface area, resulting in a higher CO production rate compared to pure g-C_3N_4. The mechanism was that Sb/g-C3N4 improved the transfer and separation efficiency of interfacial charge carriers, and the photogenerated electrons were transferred to the g-C_3N_4 conduction band during photocatalysis, with holes remaining in Sb. The electrons further reduced the CO_2 adsorbed on the catalyst surface to form CO, while the heterostructure of Sb/g-C_3N_4 promoted the desorption of the product and maintained the stability of the catalyst.[39] Zhai and colleagues explored using carbon vacancies to modify the electronic configuration of antimony atoms on carbon nitride (C_3N_4) and investigated the charge transfer process. Their density functional theory (DFT) calculations revealed a strong electronic interaction between Sb atoms and the carbon-rich vacancy C_3N_4, which helped maintain the electron-rich state of the Sb atoms and promoted photocatalytic oxygen reduction to produce H_2O_2. Their findings highlighted the importance of geometric and electronic configurations at the material interface for oxygen absorption and activation, supporting Dai's conclusions.[40] In 2023, Naveed's team pyrolyzed antimony sulfide (Sb_2S_3) nanorods using various plant oil capping agents, which demonstrated effective photocatalytic degradation of Janus Green (JG) and Rose Bengal (RB) with a degradation rate of up to 99.9%. Additionally, the activity of these nanorods remained optimal even after multiple usage cycles.[41]

In 2023, Xiao and colleagues presented antimony-substituted violet phosphorus (VP-Sb) as a photocatalyst for hydrogen evolution, showing improved stability and reduced carrier recombination.[42] Mani and his team developed a composite material of rod-shaped α-Ag_2WO_4 (n-type) modified with Sb_2S_3 (p-type) chalcogenide. The inclusion of Sb_2S_3 extended the visible light absorption of the composite compared to that of pure α-Ag_2WO_4. During photocatalytic degradation of methylene blue (MB), rhodamine B (RhB), and methyl orange (MO), the 25 wt % Sb_2S_3/α-Ag_2WO_4 nanocomposite demonstrated the highest photocatalytic degradation efficiency, suggesting its potential for treating organic pollutants in industrial wastewater.[43] Since molybdate

https://doi.org/10.1021/acsorginorgau.4c00072
ACS Org. Inorg. Au 2025, 5, 13−25

and tungstate are in the same periodic table group and share similar chemical and physical properties, modifications effective for tungstate may also apply to molybdate. Consequently, Imran's team synthesized Sb-doped cerium molybdate, which showed enhanced dielectric properties and photocatalytic activity, achieving a higher degradation rate compared to diclofenac potassium.[44]

In 2024, Imran and co-workers doped different concentrations of antimony ($Ce_{1-x}Sb_xFeO_3$, $0.00 \leq x \leq 0.09$) in $CeFeO_3$ via a coprecipitation technique to improve the photocatalytic efficiency of $CeFeO_3$. With increasing antimony concentration, the photocatalytic degradation performance of $Ce_{1-x}Sb_xFeO_3$ tended to be stable, and the degradation rate of diclofenac potassium gradually increased. As a result, $Ce_{0.93}Sb_{0.07}FeO_3$ shows the best photocatalytic activity (Table 1).[45]

Table 1. Efficiency of Photocatalytic Degradation of Potassium Diclofenac

photocatalyst	photodegradation
$CeFeO_3$	73.10%
$Ce_{0.99}Sb_{0.01}FeO_3$	75.70%
$Ce_{0.97}Sb_{0.03}FeO_3$	76.30%
$Ce_{0.95}Sb_{0.05}FeO_3$	77.00%
$Ce_{0.93}Sb_{0.07}FeO_3$	80.50%
$Ce_{0.91}Sb_{0.09}FeO_3$	75.40%

Gong and colleagues constructed a 3D/2D-hollow composite structure in situ to generate $Cs_3Sb_2I_9$ nanosheets on ZnTe microspheres. In such a stable catalyst, Te−Sb bonds improved the contacting strength at the heterojunction interface and effectively promoted charge separation. Compared to using pure ZnTe and $Cs_3Sb_2I_9$ in photocatalytic CO_2 reduction, the selectivity for CO production catalyzed by the new composite was significantly higher (from moderate to excellent).[46]

Antimony-based photocatalysts can effectively degrade toluene, rhodamine, and other compounds and reduce environmental pollution. However, the recovery and large-scale preparation of antimony-based photocatalysts are still bottlenecks restricting their industrial applications.

2.2. Applications of Antimony in Electrocatalysis

Electrocatalysis, an amalgamation of electrochemistry and homogeneous or heterogeneous catalysis, stands out as a method that enhances the efficiency and sustainability of chemical synthesis, facilitating the generation of novel molecules not easily accessible through conventional means.[47] In recent years, two-dimensional (2D) materials have become potential candidates in the realm of energy storage and transformation due to their substantial layer spacing, extensive specific surface area, and ample reactive surface and edges.[48] Antimony, identified as a 2D semiconductor with noteworthy carrier mobility, an appropriate band gap, and robust spin−orbit coupling, has garnered attention.

In 2014, Zeng's group reported the discovery of antimonene, a two-dimensional material that features a band gap of 2.28 eV and behaves as an indirect semiconductor. This property enabled the synthesis of additional semiconductor materials in the presence of group 5 elements.[49] Wang and colleagues successfully prepared single-layer antimonene on a $PdTe_2$ substrate in 2016, highlighting its substantial band gap and exceptional stability and suggesting its potential application in nanoelectronic devices.[50]

In 2018, Ebenso's team discussed nanocomposites (AONP-PANI-SWCNT) incorporating antimony oxide nanoparticles (AONPs), with polyaniline and acid-functionalized single-walled carbon nanotubes (PANI-SWCNTs) serving as supporting materials. In comparison to other glassy carbon electrode complexes, AONP-PANI-SWCNT demonstrated superior electron transport and increased electrical activity. For the electrocatalysis of lindane, the GCE-AONP-PANI-SWCNT electrode showed high sensitivity for detecting lindane even amidst various organic and inorganic interfering substances.[51]

In 2022, Cheng and his team reported on the electrocatalytic nitrogen reduction reaction (NRR) using a few-layer antimonene electrocatalyst in an aqueous K_2SO_4 electrolyte. Density functional theory (DFT) calculations demonstrated that the nitrogen reduction reaction (NRR) kinetics were enhanced by the active edges and the adsorption of hydrated potassium cations on antimonene. The main side reaction accompanying NRR is the hydrogen evolution reaction (HER). Antimony complexes and antimonate have also been demonstrated utility as catalysts in HER.[52]

Materials in thin layers exhibit better catalytic capacity, such as two-dimensional materials, which have more potential in applications than three-dimensional bulk materials. In 2017, MacFarlane's team proposed a composite of Sb nanosheets and graphene and detailed the synthesis of few-layer antimonene nanosheets (SbNSs) from bulk Sb crystals using the cathodic exfoliation method. These nanosheets were shown to be effective catalysts in the reduction of CO_2 to formate.[53] The practical catalyst was generated *in situ*; hence, it could afford large-scale processing. In 2019, Qi and co-workers utilized the high catalytic efficiency property of few-layer nanosheets and further revealed the preparation of another kind of nanometer-sized antimony, antimonene nanosheets, which had a high specific surface area that increased the number of active sites and a two-dimensional structure that increased the speed of electron transport. The structure of the antimonene nanosheets was optimized to better absorb light energy to promote light-driven water decomposition, with the material demonstrating efficient hydrogen and oxygen evolution reactions under alkaline conditions, identifying it as a catalyst with significant potential for water decomposition.[54]

Wang and colleagues revealed that the mixture of antimony doped tin oxide (ATO) combined with carbon nanotubes served as the support for a palladium catalyst (Pd/ATO-CNTs). In the electrooxidation of formic acid, the Pd/ATO-CNTs catalyst demonstrated significantly greater activity and stability compared with the Pd/CNTs catalyst. One of the reasons was that antimony-doped materials produced a large number of oxygen vacancies, making formic acid easier to oxidize.[55] Antimony-doped metal oxides are very promising catalysts for electrocatalytic oxidation as cocatalysts for Pt.

Abe's group synthesized a $Pt/NaSb_3O_7$ nanocrystal catalyst. The higher activity of $Pt/NaSb_3O_7$ in the electrocatalytic oxygen reduction reaction (ORR) under acidic conditions, compared to cutting-edge Pt-modified TiO_2 or carbon catalysts, is likely due to the enhanced electron transfer between Sb cations with different valence states. (Scheme 1).[56]

Christensen and colleagues detailed the electrocatalytic ozone generation model using Ni and Sb codoped SnO_2. They found that without Ni, Sb-doped SnO_2 could not

https://doi.org/10.1021/acsorginorgau.4c00072
ACS Org. Inorg. Au 2025, 5, 13−25

Scheme 1. Electron-Hopping Model for the Enhanced ORR Activity of Pt/$NaSb_3O_7$

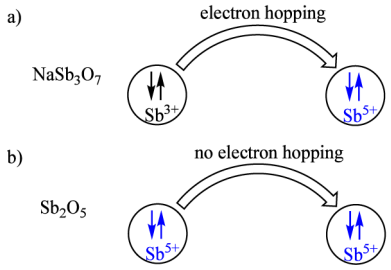

generate ozone electrocatalytically, highlighting a synergistic interaction between Ni and Sb. Sb(V) enhanced the electronic conductivity of SnO_2, while the incorporation of Ni(II) created oxygen vacancies that facilitated the dissociation of adsorbed molecular oxygen into single oxygen atoms at the Sb(III) sites. These atoms then reacted with adsorbed hydroxyl molecules to form ozone.[57] To address the issue of the short service life of SnO_2-Sb electrodes in wastewater degradation, Zhang and colleagues developed a Nb-TiO_2 nanotube (Nb-Ti/Nb-TiO_2-NTs/ATONPs) electrode for the electrocatalytic degradation of Acid Red 73. They found that the electrochemical oxidation performance of Nb-Ti/Nb-TiO_2-NTs/ATONPs surpassed that of Ti-based electrodes with an energy consumption reduction of 28.8%. The loading of Nb−TiO_2 nanotubes created channels for mass transfer, leading to the improvement of the adsorption capacity and charge transfer efficiency of the novel composites.[58]

In 2023, Li and his team fabricated Sb-doped SnO_2/Ti electrodes and studied their effectiveness in the electrocatalytic degradation of RhB. The degradation rate of the electrode reached 99.1% after 150 min in an alkaline medium via the Sb-doped electrode. This kind of electrode showed high stability and repeatability and initiated hydroxyl radicals (•OH) to react and to decompose RhB in alkaline solution. The degradation intermediates of RhB were identified using HPLC-MS, which allowed for the hypothesized degradation pathway of RhB to be proposed (Scheme 2).[59] In the electrocatalysis process, the hydroxyl group adsorbed on the electrode surface will not only generate •OH to degrade RhB but also form Sn−OH with Sn. •OH can also promote the conversion of Sn−OH to SnO_2, thereby restoring the activity and stability of the electrode. The presence of Sb provides additional free electrons for SnO_2, narrows the band gap of SnO_2, and makes the electrode more inclined to produce •OH than the electrode with O_2.

In 2017, Zhu et al. applied a sol−gel method to coat nano-Sb-doped SnO_2 (Sb-SnO_2) onto a polyporous coal-based carbon film (CM). The Sb−SnO_2 was evenly distributed across the CM surface and securely bonded through C−O−Sn chemical bonds, which improved the stability of the coating. The resulting Sb-SnO_2/CM exhibited a high oxygen evolution potential (OEP), strong electrocatalytic activity, and durability. It also retained excellent conductivity, leading to better electrocatalytic degradation of tetracycline compared to the uncoated CM.[60]

In 2018, Yu et al. developed an Sb−Ni cyanogel by reacting $SbCl_3$ with $K_2Ni(CN)_4$. This cyanogel was subsequently reduced to create a 3D Sb−Ni alloy framework, resulting in a consistent Sb−Ni−C ternary anode. The Sb−Ni−C anode, enhanced with two-dimensional reduced graphene oxide

Scheme 2. Possible Electrochemical Degradation Pathways of RhB

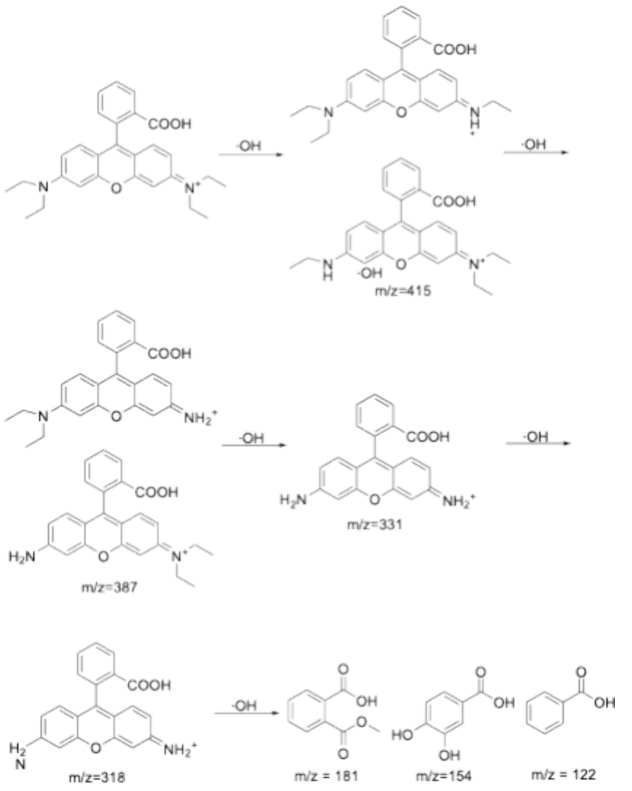

(rGO) carbon, exhibited excellent durability and effectively mitigated the problem of substantial volume expansion during operation.[61]

In 2022, Nørskov's group developed antimonate (MSb_2O_6, M = Fe, Co, Ni, and Mn) with commendable electrical conductivity, thermodynamic stability, and aqueous stability in basic conditions (pH = 13). The study highlighted that $MnSb_2O_6$ proved to be the most efficient catalyst for facilitating the oxygen reduction reaction. Additionally, it was found that antimonate could function as a framework to modify the catalytic properties of transition metal oxides, including NiO.[62] In 2023, Kang and co-workers enhanced the efficiency and stability of antimony oxide on the surface of Pt nanoparticles (SbO_x-Pt) in the electrochemical glycerin catalytic oxidation reaction (EGOR). The deposition of SbO_x changed the absorption of the Pt electrocatalyst. Compared to Pd/C, the modified catalyst had high selectivity for the production of dihydroxyacetone and a high cyclo-rate.[63] Huang and colleagues created ultrathin antimony oxide-coated Ir−Sb nanowires (Ir−Sb NWs/SbO_x) as highly effective bifunctional catalysts for the hydrogen oxidation reaction (HOR) and hydrogen evolution reaction (HER) under alkaline conditions. Compared with Ir NW/C and commercial Pt/C, the Ir−Sb NW/SbO_x nanowires displayed superior catalytic performance. The study highlights that the ultrathin structure and the presence of Sb sites occupied by H_2O enhance the inherent catalytic activity of Ir and significantly improve OH* absorption during alkaline HER/HOR electrolysis. In addition, the protection brought by the SbO_x layer further prevented poisoning from carbon monoxide.[64]

In 2021, Hisaeda's group synthesized and characterized the novel porphyrin antimonate complexes Sb(III)OEPo and

https://doi.org/10.1021/acsorginorgau.4c00072
ACS Org. Inorg. Au 2025, 5, 13−25

Scheme 3. Synthesis of Porphycene Antimony Complexes

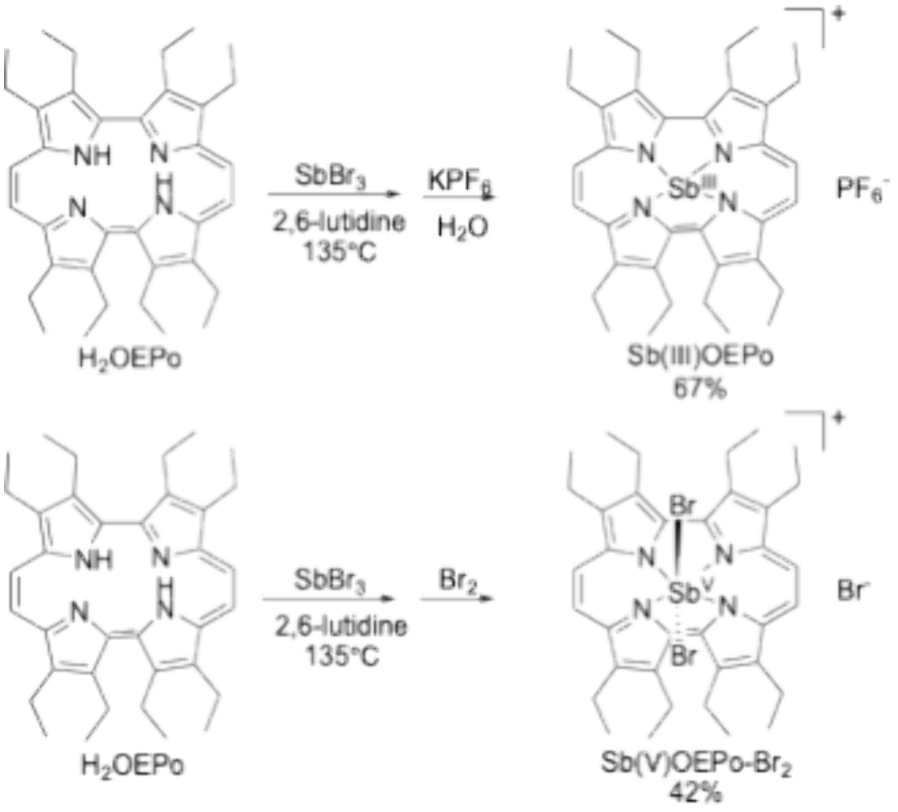

Sb(V)OEPO-Br_2 (Scheme 3). The hydrogen evolution reaction was driven by the reduction of the antimony porphyrin at the center of the ligand, and the redox property of the porphyrin allowed antimony to act as the central element of the complex caused by the anodically shifted condition.[65]

In 2024, Si and colleagues first explored the use of an antimony corrole in HER. They prepared three novel antimony corroles featuring nitro groups located at the *ortho-*, *meta-*, and *para*-positions of the 10-phenyl group (Figure 4a). The hydrogen evolution reaction (HER) performance of these corroles was assessed in acetonitrile and a neutral buffer solution (V_{DMF}/V_{H2O} = 1:2). Both solvents demonstrated significant electrocatalytic HER activity, although the activity tended to diminish from 3 to 5. They proposed that the catalytic process for antimony involves the assistance of two proton sources: TFA and TsOH (Figure 4b). The proposed mechanism includes the antimony corrole complex binding two protons, followed by the release of hydrogen gas.[66]

In 2017, Crabtree's team developed a range of antimony porphyrin complexes, and TPSb$(OH)_2$ was extensively examined to confirm its catalytic effectiveness. Density functional theory (DFT) results demonstrated its potential as a proton reduction catalyst.[67] Conversely, Cheng's research indicated that potassium cations hindered proton movement within the interfacial water layer, thus prioritizing nitrogen reduction reactions (NRR) over hydrogen evolution reactions (HER).[52]

Meanwhile, Zhou's team synthesized a novel complex salt by combining an organic hybrid dysprosium cation with chalcogenidoantimonate as the counterion. This complex was produced by reacting Sb, Se, $DyCl_3$, and triethylene tetramine

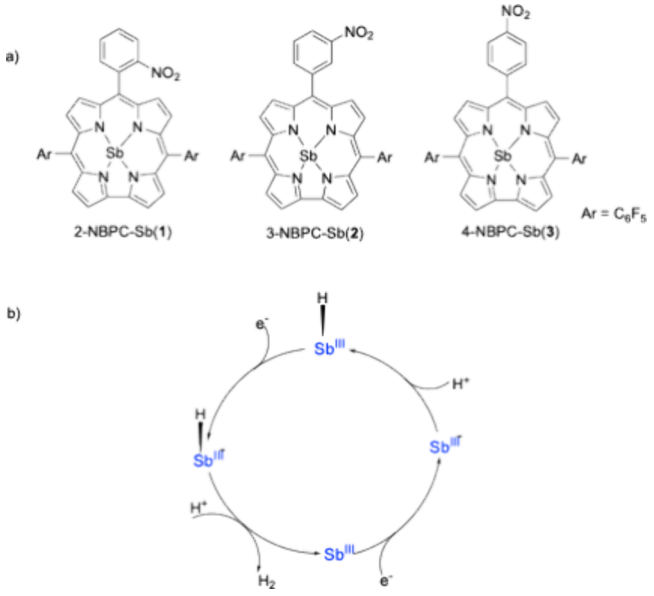

Figure 4. (a) Structures of the three antimony corrole complexes. (c) Proposed catalytic cycle of HER with Sb corroles.

(teta) at 170 °C for a week. The researchers then assembled Ni/SbSe-1@AB/NF electrodes by integrating SbSe-1 with acetylene black (AB), nickel nanoparticles, and porous nickel foam (NF). These electrodes were utilized as electrocatalysts for the oxygen evolution reaction (OER), showcasing excellent catalytic performance due to the combined effects of SbSe-1, AB, and nickel nanoparticles (Figure 5).[68]

Ma's team successfully developed a carbon-supported Sb/Bi bimetallic composite for electrocatalytic CO_2 reduction. They

https://doi.org/10.1021/acsorginorgau.4c00072
ACS Org. Inorg. Au 2025, 5, 13−25

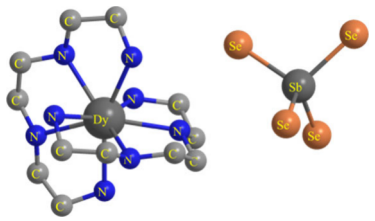

Figure 5. 3D structure of $[Dy(teta)_2][SbSe_4]$.

discovered that the addition of a small amount of Sb improved both the stability of the electrode and the selectivity for formate production in Bi-based materials. The presence of Sb notably reinforced the physical structure of the carbon spheres on the surface of the composite and effectively prevented their dissolution, thus reducing the degradation of Bi materials.[69]

2.3. Applications of Antimony in Organic Synthesis

Olah et al. proposed that fluoro-antimonic acid represents a robust Lewis acid, with its acidity reaching $H_0 = -28$ in the case of 1:1 HF/SbF_5. It was even stronger than Magic Acid (HSO_3F/SbF_5, $H_0 = -15.1$). The replacement of SbF_5 with other Lewis acids tended to diminish the acidity. Fluoro-antimonic acid, characterized as a potent Lewis acid, could protonate supersaturated hydrocarbons and readily protonated (or coordinated with) unbonded electron pair donors. The broad protonation scope underscored the capacity of antimony to represent an extremely strong Lewis acid.[70]

In 2014, Gabbaï's group synthesized antimony triflate derivative **5** and stibonium borate salt $[Sb(C_6F_5)_4][B(C_6F_5)_4]$ **6** starting from $SbCl(C_6F_5)_4$ **4** (Scheme 4a). Ion-pair complex **6** exhibited rather strong Lewis acidity, which could even attract a fluorine anion from $[SbF_6]^-$ and $[BF(C_6F_5)_3]^-$. It was applied in the polymerization of THF and the hydro-

Scheme 4. Synthesis of Antimony Lewis Acid Derivative and Application of Hydrosilylation of Benzaldehyde

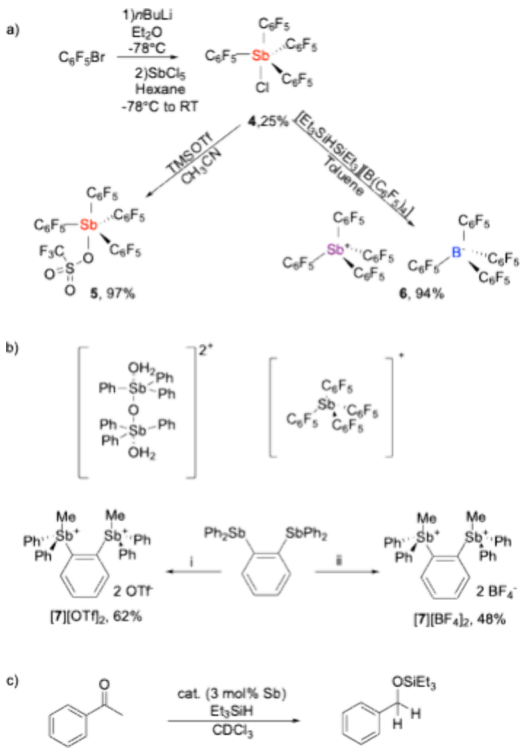

defluorination reaction of fluorothane, showcasing its robust Lewis acid character. The tetrahedral arrangement of the Sb center hinders approach of the nucleophile, contributing to its stability even in air conditions. Basically, in the preliminary exploration of stibonium borate salt complex, it had great potential in replacing reagents with Lewis acidic functions in more reactions.[71] In 2016, Gabbaï's group continued to construct novel stibonium structures. This time, they utilized $[1,2\text{-}(Ph_2MeSb)_2C_6H_4]^{2+}$($[7]^{2+}$) to prepare $[7][OTf]_2$ and $[7][BF_4]_2$ (Scheme 4b), revealing its potential ability in double-activation of the carbonyl functional group under mild conditions. In the selected reaction model, stibonium salt was designed to catalyze the hydrosilanization of benzaldehyde (Scheme 4c).[72]

Gabbaï and colleagues prepared another fluorinated stiborane derivative with Lewis acidity close to that of $B(C_6F_5)_3$. They selected $Sb(C_6F_5)_3$ as starting material to react with *o*-chloranil, and then the designed product $Sb(C_6F_5)_3(O_2C_6Cl_4)$ was obtained efficiently in high purity. They found the novel Lewis acid could react with phosphines to access frustrated Lewis pairs (FLPs). With the reaction property in hand, they continued to utilize $o\text{-}C_6H_4(PPh_2)(SbCl_2)$ to synthesize a FLP with a strong intramolecular interaction by mimicking the same preparation method (Scheme 5). The closer distance increased the interaction between P and Sb, which made the complex significantly inert to water. Hence, the ambiphilic FLP was successfully applied to reaction of formaldehyde in aqueous solution, demonstrating the novel FLP with strong Lewis acidic energy and water tolerance had a wide range of applications.[73]

To increase the Lewis acidity of the antimony cation, Gabbaï devised and incorporated a second cationic center, finding that bicationic derivatives showed the highest catalytic efficiency in the reduction of quinoline by Hantzsch ester (Scheme 6).[9] The parallel comparison result showed that the stibonium ion had stronger Lewis acidity than the phosphonium ion. Thus, distibonium complex **13** gave the best performance in the hydrogenation reaction.

Most recently, Gabbaï's group discovered that 5-phenyl-5,5-dichloro-λ^5-dibenzostibole **14** displayed higher Lewis acidity than Ph_3SbCl_2 and Mes_3SbCl_2. By imposing geometric constraints, **14** demonstrated enhanced performance and served as a catalyst for the reduction of quinoline and imine (Scheme 7).[74] The authors conducted DFT calculations to reveal the relationship between function and structure. In their study, compared to Ph_3SbCl_2, the five-membered heterocycle ring constructed within the antimony center changed the geometry of complex and left a larger σ-hole in the equatorial orbital. Consequently, the Lewis acid had more contact with the substrates and showed better catalytic performance. To date, Gabbaï's group has ceased merely creating and studying new structures of antimony reagents. They observed the working principles of antimony complexes as Lewis acids and applied them in various reactions. Due to antimony's high Lewis acidity, they explored the use of organic antimony compounds as new platforms for trapping, sensing, and transporting anions, of which encoding a photophysical response and transporting an anion across the biological phospholipid membranes were promising.[75]

The two-centered Lewis acid gained success and attracted a lot of attention from chemists. Gabbaï's team prepared various antimony cations and assessed their catalytic effectiveness in cycloaddition reactions involving isocyanates and oxiranes. The

https://doi.org/10.1021/acsorginorgau.4c00072
ACS Org. Inorg. Au 2025, 5, 13−25

Scheme 5. Preparation of Ambiphilic Phosphino-stiboranes

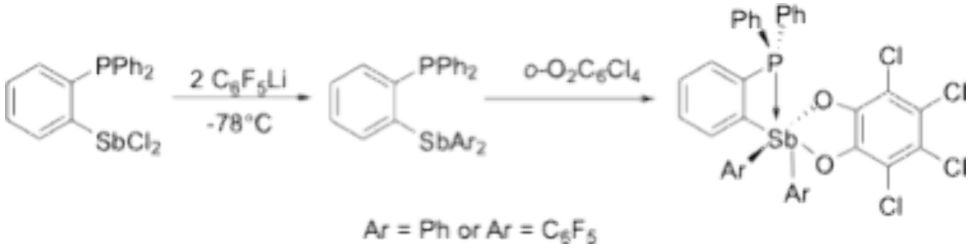

Scheme 6. Mono- and Bicationic Phosphorus and Antimony Lewis Acid Derivatives and the Hydrogenation of Quinolines Catalyzed by Different Distibonium Complexes

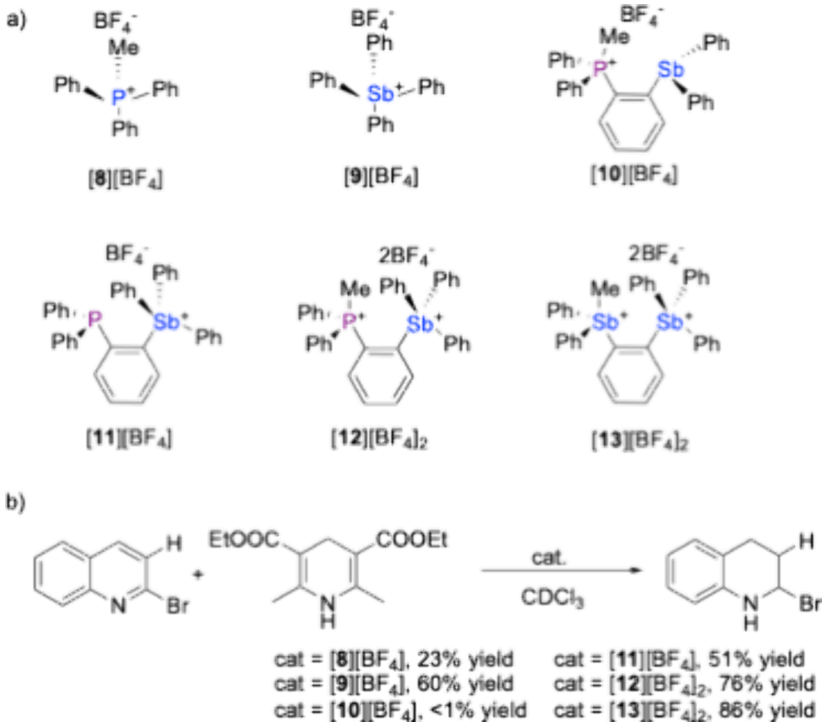

Scheme 7. Solid-State and Solution Structure of 14 and its THF Adduct Used in Transfer Hydrogenation Reactions

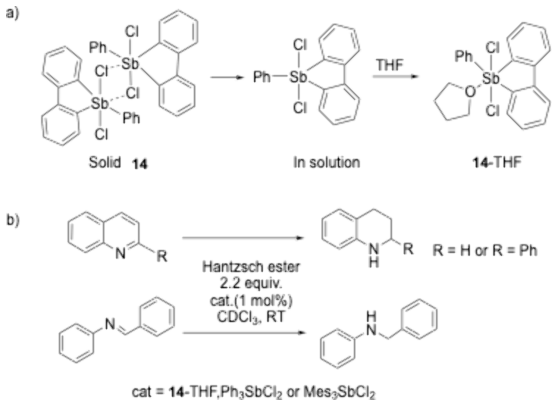

lower catalytic activity of antimony ions (19^+ and 20^+) can be ascribed to the contribution of nitrogen atoms from the intramolecular dimethylamino group due to the reduction in Lewis acidity caused by the antimony atom. The bulky antimony ion (16^+−18^+) as well as the electron-rich isocyanate increase the regional selectivity of the reaction, which is best at catalyst 18^+ in favor of the 3,4-isomer (**A**). Finally, without the presence of the Sb catalyst, the reaction proceeded slowly and produced only **B** as the main product (Scheme 8).[76]

Scheme 8[a]

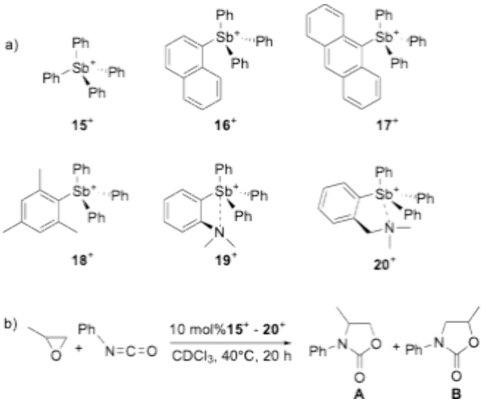

[a](a) Various tetraarylstibonium ions. (b) Antimony ion-catalyzed cycloaddition reaction between propylene oxide and phenyl isocyanate.

https://doi.org/10.1021/acsorginorgau.4c00072
ACS Org. Inorg. Au 2025, 5, 13−25

Qiu's group also synthesized a range of organoantimony(III) halide complexes. These complexes featured a tetrahydrodibenzo[*c*,*f*][1,5]azastibocine framework, where a donor−acceptor interaction between the nitrogen and antimony atoms influenced the catalytic activity of antimony. Conversely, the halogen bonded to the antimony center operated in a push−pull manner to modulate the Lewis acidity. The combined effects of the nitrogen substituents and halogen atoms around the central antimony(III) atom created Lewis acid catalysts for various reactions, including the Mannich reaction, cross-condensation, cyclization-aromatization, and aminolysis of epoxides. Among these, fluorinated organoantimony(III) derivatives demonstrated higher activity compared to their chlorinated, brominated, and iodinated counterparts, as the Sb−F moiety acted as a more effective hydrogen bond acceptor. (Scheme 9). The Sb−F moiety showed better catalytic efficiency and could be recycled and reused.[77]

Scheme 9. Preparation of Organoantimony(III) Compounds

Yin and his colleagues applied the diantimony-centered strategy to design and synthesize a novel bimetallic organic antimony catalyst, which had four Lewis/Brønsted acidic/basic sites (Scheme 10). It was used in the diastereoselective direct Mannich reaction and showed a high catalytic efficiency (catalyst load of 0.1%).[78]

Scheme 10. Synthesis of a Bimetallic Organic Antimony Catalyst

In the field of asymmetric catalysis, Tan's group achieved a breakthrough in 2021. Utilizing chiral mandelic acid derivative **22** as the chiral source, they synthesized chiral antimony compound **23** and chiral antimony anion/cation pair **24**. The active species in the reduction of benzoxazine by Hantzsch ester was identified as **24**, exhibiting high efficiency and selectivity with good compatibility across substrates with different substituents (Scheme 11).[79] In 2022, Pupkova and co-workers discovered a photodegradation application of an ionic complex formed by 3,5-dinitrosalicylic acid and pentaphenylantimony.[80]

In 2016, Zhang's group prepared antimony-doped CeO_2-WO_3/TiO_2 catalyst and used it for the catalytic reduction of NO_x. Adding Sb to CeO_2-WO_3/TiO_2 greatly enhanced the selective catalytic reduction of NH_3 at lower temperatures. Among the catalysts, $Sb_5Ce_{10}W_6$/Ti had better low-temperature catalytic activity, which was of certain significance for the development of an NH_3 denitrification catalyst.[81]

Scheme 11. Synthesis of a Chiral Antimony(V) Cation/Anion Pair

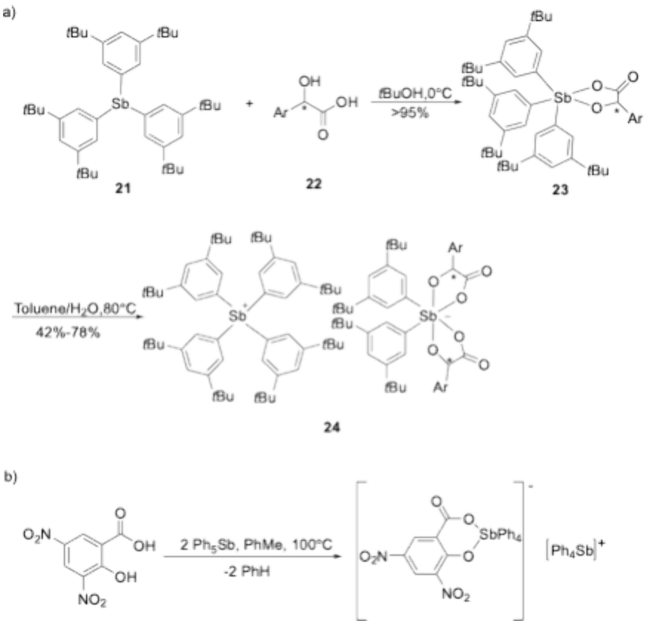

Wang's group isolated a new polymolybdoxide containing antimonium $[(CH_3)_4N]_6H[Sb^{V}Sb^{III}{}_4Mo_{18}O_{66}]\cdot 9H_2O$ in aqueous solution. This compound was then used as a heterogeneous catalyst to convert organosilanes to silane alcohols under gentle reaction conditions. Single crystal X-ray revealed the exact three-layered structure of the polyheteromolybdate scaffold with antimonate. The middle layer of the oxygen-bridge bond connected the antimonate layer and the molybdate layer. Moreover, the catalyst still retained its catalytic activity after three reaction cycles.[82]

Narasimharao and co-workers synthesized a Sb-implanted Keggin-structured ammonium salt of 12-molybdophosphoric acid (AMPA) catalyst. The number of Sb atoms increased from 1 to 3, while the Mo atoms were replaced accordingly (from 11 to 9). It was used to catalyze the chlorobenzene gas-phase oxidation reaction (Scheme 12), and the catalytic

Scheme 12. Sb-AMPA Catalyzes Chlorobenzene Oxidation

performance was assessed relative to the original AMPA sample. Sb doping increased the thermal stability of AMPA and improved the conversion of chlorobenzene, likely due to more Sb−O−Mo species being present in the catalyst.[83]

The oxidations mentioned in photo- and electrocatalysis are usually used in water splitting and the degradation of organic pollutions. Most recently, Huang and co-workers mixed Sb_2O_3 and Cu^{2+} ions to form Sb_2O_3−CuO nanocomposites through microwave heating, which were used for the catalytic degradation of *p*-nitrophenol (PNP). When Sb_2O_3−CuO nanocomposites were mixed into PNP, the UV−vis absorbance of PNP was reduced significantly in 3 s, while the other materials did not show a similar performance. The Sb_2O_3−CuO nanocomposite can efficiently degrade the PNP, with a degradation rate of 96% (Scheme 13).[84]

https://doi.org/10.1021/acsorginorgau.4c00072
ACS Org. Inorg. Au 2025, 5, 13−25

Scheme 13. Proposed Degradation Pathways of PNP by the Sb_2O_3−CuO Catalyst

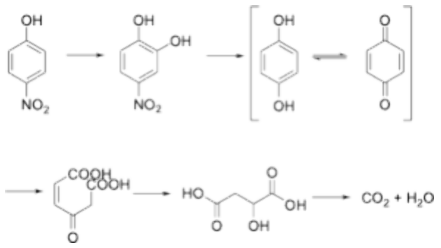

Inspired by N_3/CX and C_3/CN types of click reactions, Manners and colleagues designed a P_3/CN type of click reaction and aimed to obtain a series of stable 1-aza-2,3,4-triphospholenes (Scheme 14). They employed organoantimo-

Scheme 14. Dipolar Additions of N_3, C_3, and P_3 Frameworks with CX Triple Bonds

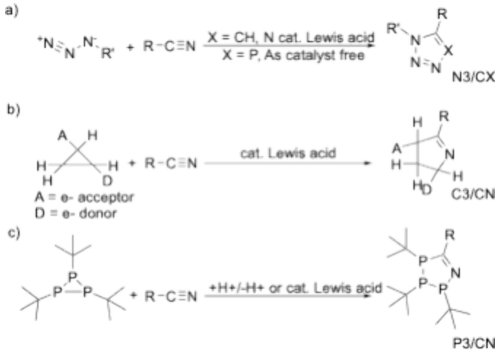

nide $Ph_3SbCl(OTf)$ and $Ph_3Sb(OTf)_2$ as the optimal Lewis acid catalysts for the addition of cyclophosphine to nitriles, yielding the desired product with high selectivity in a broader scope.[85]

In 2020, Matile's group reported the pnictogen bonding catalysis applied in epoxy-ring-opening polyether cyclization, which led to an anti-Baldwin product. They demonstrated distinct regional and stereoselectivity between Sb(III) and high-valence Sb(V) catalysts and explained how the epoxide substrate occupied the σ-hole to give anti-Baldwin cyclization adducts.[86]

Garcia and colleagues prepared thin films containing antimony oxide nanoparticles (SbOx/fl-G and SbOx/fl-(N)G) on quartz using $Sb(OAc)_3$ adsorbed by alginate or chitosan, and the material can be used as a catalyst to promote the Michael addition of active methylene to conjugated enones (Scheme 15a) and Henry condensation between nitromethane and benzaldehyde (Scheme 15b). Compared with SbOx/fl-G, SbOx/fl-(N)G shows better catalytic activity and selectivity and improves the conversion rate of the reaction.[87]

3. CONCLUSION

In summary, in the fields of photocatalysis and electrocatalysis, the mechanisms are generally similar in their respective applications, where electrons are moved by light or electricity. Antimony and its derivatives added to composite materials or electrodes have a stronger electron conduction ability compared to the raw materials or original electrodes, enabling them to exhibit outstanding performance in wastewater treatment and carbon dioxide reduction and utilization,

Scheme 15. SbOx/fl-G- and SbOx/fl-(N)G-Catalyzed Michael Addition and Henry Addition

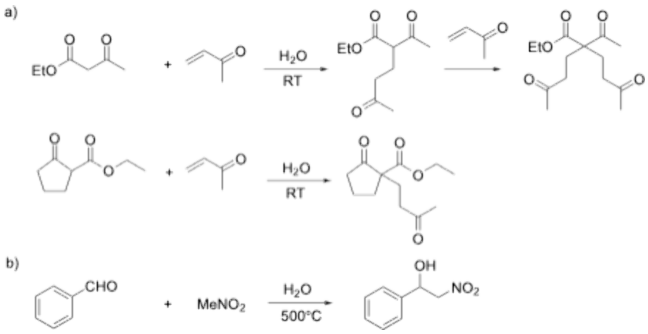

among other applications. For example, in wastewater treatment, research objects include the degradation of rhodamine B, aniline, Janus Green, and Rose Bengal, among other organic pollutants. In carbon dioxide recovery and utilization, carbon dioxide can be reduced to carbon monoxide or converted to formic acid salts for immobilization. In other organic synthesis fields, the mainstream research focuses on the evolution of ultrastrong Lewis acid catalysts, where the reactions can be comparable to or even surpass those catalyzed by classic Lewis catalysts represented by boron compounds. Recently, there has been one example of an ion pair catalytic reaction combined with chiral mandelic ligands, where antimony exhibits catalytic effects similar to those of the phosphorus element in the same family. In cases where it is combined with other metals, antimony more often displays its metallic properties while maintaining the original properties of the compound and enhancing the stability of the original catalyst, thereby increasing the number of cycles and reducing losses. In the future, we believe that the more mature experience in photo/electrocatalysis can be further expanded and applied to other organic reactions, making antimony the main functional source of catalysis and expanding the knowledge interface of antimony in the field of organic chemistry.

■ ASSOCIATED CONTENT

Data Availability Statement

The data underlying this study are available in the published article.

■ AUTHOR INFORMATION

Corresponding Authors

Choon-Hong Tan − *School of Chemistry, Chemical Engineering and Biotechnology, Nanyang Technological University, Singapore 637371, Singapore;* orcid.org/0000-0003-3190-7855; Email: choonhong@ntu.edu.sg

Xinyi Ye − *College of Pharmaceutical Science & Collaborative Innovation Center of Yangtze River Delta Region Green Pharmaceuticals, Zhejiang University of Technology, Hangzhou 310014, P. R. China;* orcid.org/0000-0002-5344-9122; Email: xinyiye1020@zjut.edu.cn

Author

Lewen Wu − *College of Pharmaceutical Science & Collaborative Innovation Center of Yangtze River Delta Region Green Pharmaceuticals, Zhejiang University of Technology, Hangzhou 310014, P. R. China*

https://doi.org/10.1021/acsorginorgau.4c00072
ACS Org. Inorg. Au 2025, 5, 13−25

Complete contact information is available at:
https://pubs.acs.org/10.1021/acsorginorgau.4c00072

Author Contributions

CRediT: **Lewen Wu** writing - original draft.

Notes

The authors declare no competing financial interest.

■ ACKNOWLEDGMENTS

We gratefully acknowledge the National Key Research & Development Program of China (no. 2023YFA1506403) and the National Natural Science Foundation of China (no. 22101255) for financial support.

■ ABBREVIATIONS

ATO, antimony-doped tin oxide; RhB, rhodamine B; POPD, poly(*o*-phenylenediamine); MB, methylene blue; MO, methyl orange; AONP, antimony oxide nanoparticles; SbNSs, antimonene nanosheets; CNTs, carbon nanotubes; NRR, nitrogen reduction reaction; HER, hydrogen evolution reaction; ORR, oxygen reduction reaction; CM, carbon film; OEP, oxygen evolution potential; rGO, reduced graphene oxide; EGOR, electrochemical glycerin catalytic oxidation reaction; HOR, hydrogen oxidation reaction; AB, acetylene black; NF, nickel foam; AMPA, ammonium salt of 12-molybdophosphoric acid; PNP, *p*-nitrophenol

■ REFERENCES

(1) Girolami, S. G. Origin of the Terms Pnictogen and Pnictide. *J. Chem. Educ.* **2009**, *86*, 1200−1201.
(2) Damhus, T.; Hartshorn, R. M.; Hutton, A. T. Nomenclature of Inorganic Chemistry-IUPAC Recommendations 2005. *Chem. Int.* **2005**, *27*, 25−26.
(3) Hirai, M.; Cho, J.; Gabbaï, F. P. Promoting the Hydrosilylation of Benzaldehyde by Using a Dicationic Antimony-Based Lewis Acid: Evidence for the Double Electrophilic Activation of the Carbonyl Substrate. *Chem.-Eur. J.* **2016**, *22*, 6537−6541.
(4) Liu, C.; Shin, J.; Son, S.; Choe, Y.; Farokhzad, N.; Tang, Z.; Xiao, Y.; Kong, N.; Xie, T.; Kim, J. S.; Tao, W. Pnictogens in medicinal chemistry: evolution from erstwhile drugs to emerging layered photonic nanomedicine. *Chem. Soc. Rev.* **2021**, *50*, 2260−2279.
(5) Angarov, V.; Kozuch, S. On the σ, π and δ hole interactions: a molecular orbital overview. *New. J. Chem.* **2018**, *42*, 1413−1422.
(6) Murray, J. S.; Lane, P.; Clark, T.; Politzer, P. σ-hole bonding: molecules containing group VI atoms. *J. Mol. Model.* **2007**, *13*, 1033−1038.
(7) Feng, X.; Du, H. Asymmetric Transfer Hydrogenation via a Chiral Antimony (V) Cation/Anion Pair. *Chinese. J. Org. Chem.* **2021**, *41*, 3335−3336.
(8) Pan, B.; Gabbaï, F. P. $[Sb(C_6F_5)_4][B(C_6F_5)_4]$: an air stable, Lewis acidic stibonium salt that activates strong element-fluorine bonds. *J. Am. Chem. Soc.* **2014**, *136*, 9564−9567.
(9) Yang, M.; Hirai, M.; Gabbaï, F. P. Phosphonium−stibonium and bis-stibonium cations as pnictogen-bonding catalysts for the transfer hydrogenation of quinolines. *Dalton. Trans.* **2019**, *48*, 6685−6689.
(10) Li, N.; Qiu, R.; Zhang, X.; Chen, Y.; Yin, S. F.; Xu, X. Strong Lewis acids of air-stable binuclear triphenylantimony (V) complexes and their catalytic application in C−C bond-forming reactions. *Tetrahedron.* **2015**, *71*, 4275−4281.
(11) Berry, F. J. Tin–antimony oxide oxidation catalysts. *Hyperfine Interact.* **1998**, *111*, 35−37.
(12) Varadwaj, A.; Varadwaj, P. R.; Marques, H. M.; Yamashita, K. The Stibium Bond or the Antimony-Centered Pnictogen Bond: The Covalently Bound Antimony Atom in Molecular Entities in Crystal Lattices as a Pnictogen Bond Donor. *Int. J. Mol. Sci.* **2022**, *23*, 4674.
(13) Mamta; Singh, Y.; Maurya, K. K.; Singh, V. N. A review on properties, applications, and deposition techniques of antimony selenide. *Sol. Energy Mater. Sol. C* **2021**, *230*, No. 111223.
(14) Wang, X.; Song, J.; Qu, J. Antimonene: From Experimental Preparation to Practical Application. *Angew. Chem., Int. Ed.* **2019**, *58*, 1574−1584.
(15) Tao, W.; Ji, X.; Xu, X.; Islam, M. A.; Li, Z.; Chen, S.; Saw, P. E.; Zhang, H.; Bharwani, Z.; Guo, Z.; Shi, J.; Farokhzad, O. C. Antimonene Quantum Dots: Synthesis and Application as Near-Infrared Photothermal Agents for Effective Cancer Therapy. *Angew. Chem., Int. Ed.* **2017**, *56*, 11896−11900.
(16) Liu, D. Y.; Li, H. Y.; Han, R. P.; Liu, H. L.; Zang, S. Q. Multiple Stimuli-Responsive Luminescent Chiral Hybrid Antimony Chlorides for Anti-Counterfeiting and Encryption Applications. *Angew. Chem., Int. Ed.* **2023**, *62*, No. e202307875.
(17) Fagnoni, M.; Protti, S.; Ravelli, D. Photoorganocatalysis in Organic Synthesis. *Catal. Sci. Series* **2019**, *18*, 471−518.
(18) Sideri, I. K.; Voutyritsa, E.; Kokotos, C. G. Photo-organocatalysis, small organic molecules and light in the service of organic synthesis: the awakening of a sleeping giant. *Org. Biomol. Chem.* **2018**, *16*, 4596−4614.
(19) Akita, M.; Ceroni, P.; Stephenson, C. R. J.; Masson, G. Progress in Photocatalysis for Organic Chemistry. *J. Org. Chem.* **2023**, *88*, 6281−6283.
(20) Guo, Q.; Zhou, C.; Ma, Z.; Yang, X. Fundamentals of TiO_2 Photocatalysis: Concepts, Mechanisms, and Challenges. *Adv. Mater.* **2019**, *31*, No. 1901997.
(21) Prier, C. K.; Rankic, D. A.; MacMillan, D. W. Visible light photoredox catalysis with transition metal complexes: applications in organic synthesis. *Chem. Rev.* **2013**, *113*, 5322−5363.
(22) Sato, S.; Morikawa, T.; Kajino, T.; Ishitani, O. A highly efficient mononuclear iridium complex photocatalyst for CO_2 reduction under visible light. *Angew. Chem., Int. Ed.* **2013**, *52*, 988−992.
(23) Lee, S. Y.; Park, S. J. TiO_2 photocatalyst for water treatment applications. *J. Ind. Eng. Chem.* **2013**, *19*, 1761−1769.
(24) Tolosana-Moranchel, A.; Pecharromán, C.; Faraldos, M.; Bahamonde, A. Strong effect of light scattering by distribution of TiO_2 particle aggregates on photocatalytic efficiency in aqueous suspensions. *Chem. Eng. J.* **2021**, *403*, No. 126186.
(25) Tobaldi, D. M.; Dvoranová, D.; Lajaunie, L.; Rozman, N.; Figueiredo, B.; Seabra, M. P.; Škapin, A. S.; Calvino, J. J.; Brezová, V.; Labrincha, J. A. Graphene-TiO_2 hybrids for photocatalytic aided removal of VOCs and nitrogen oxides from outdoor environment. *Chem. Eng. J.* **2021**, *405*, No. 126651.
(26) Chen, L.; Chen, P.; Wang, H.; Cui, W.; Sheng, J.; Li, J.; Zhang, Y.; Zhou, Y.; Dong, F. Surface Lattice Oxygen Activation on $Sr_2Sb_2O_7$ Enhances the Photocatalytic Mineralization of Toluene: from Reactant Activation, Intermediate Conversion to Product Desorption. *ACS. Appl. Mater. Interfaces.* **2021**, *13*, 5153−5164.
(27) Luo, L.; Li, T.; Ran, X.; Wang, P.; Guo, L. Probing Photocatalytic Characteristics of Sb-Doped TiO_2 under Visible Light Irradiation. *J. Nanomater.* **2014**, *2014*, No. 947289.
(28) Zhou, H.; Ge, J.; Zhang, M.; Yuan, S. Photoelectrocatalytic properties of TiO_2/ATO composite films. *Res. Chem. Intermed.* **2016**, *42*, 1929−1941.
(29) Yamaguchi, Y.; Usuki, S.; Yamatoya, K.; Suzuki, N.; Katsumata, K. I.; Terashima, C.; Fujishima, A.; Kudo, A.; Nakata, K. Efficient photocatalytic degradation of gaseous acetaldehyde over ground Rh-Sb co-doped $SrTiO_3$ under visible light irradiation. *RSC. Adv.* **2018**, *8*, 5331−5337.
(30) Zhao, H.; Tang, J.; Lai, Q.; Cheng, G.; Liu, Y.; Chen, R. Enhanced visible light photocatalytic performance of Sb-doped $(BiO)_2CO_3$ nanoplates. *Catal. Commun.* **2015**, *58*, 190−194.
(31) Chen, J.; Li, D.; Wang, J.; Wang, P.; Cao, C.; Shao, Y.; Wang, J.; Xian, J. Morphological effect on photocatalytic degradation of Rhodamine B and conversion of active species over $BaSb_2O_6$. *Appl. Catal., B* **2015**, *163*, 323−329.

(32) Kong, L.; He, M.; Hu, X. Rapid photooxidation of Sb(III) in the presence of different Fe(III) species. *Geochim. Cosmochim. Ac.* **2016**, *180*, 214−226.
(33) Nasser, R.; Othmen, W. B. H.; Elhouichet, H.; Férid, M. Preparation, characterization of Sb-doped ZnO nanocrystals and their excellent solar light driven photocatalytic activity. *Appl. Surf. Sci.* **2017**, *393*, 486−495.
(34) Huerta-Flores, A. M.; Torres-Martínez, L. M.; Moctezuma, E.; Carrera-Crespo, J. E. Novel $SrZrO_3$-Sb_2O_3 heterostructure with enhanced photocatalytic activity: Band engineering and charge transference mechanism. *J. Photoch. Photobio. A* **2018**, *356*, 166−176.
(35) Barrio, J.; Gibaja, C.; Tzadikov, J.; Shalom, M.; Zamora, F. 2D/2D Graphitic Carbon Nitride/Antimonene Heterostructure: Structural Characterization and Application in Photocatalysis. *Adv. Sustain. Syst.* **2019**, *3*, No. 1800138.
(36) Al-Namshah, K. S.; Mohamed, R. M. Silver-Doped Antimony Trioxide Nanocomposites for the Photocatalytic Reduction of Nitrobenzene. *J. Nanosci. Nanotechnol.* **2019**, *19*, 3528−3535.
(37) Zia, J.; P, M. R.; Riaz, U. Photocatalytic degradation of anti-inflammatory drug using POPD/Sb_2O_3 organic-inorganic nanohybrid under solar light. *J. Mater. Res. Technol.* **2019**, *8*, 4079−4093.
(38) Kokabi, A.; Touski, S. B. Electronic and photocatalytic properties of Antimonene nanosheets. *Physica. E* **2020**, *124*, No. 114336.
(39) Zhang, J.; Fu, J.; Dai, K. Graphitic carbon nitride/antimonene van der Waals heterostructure with enhanced photocatalytic CO_2 reduction activity. *J. Mater. Sci. Technol.* **2022**, *116*, 192−198.
(40) He, Q.; Ding, J.; Tsai, H. J.; Liu, Y.; Wei, M.; Zhang, Q.; Wei, Z.; Chen, Z.; Huang, J.; Hung, S. F.; Yang, H.; Zhai, Y. Boosting photocatalytic hydrogen peroxide production by regulating electronic configuration of single Sb atoms via carbon vacancies in carbon nitrides. *J. Colloid Interface Sci.* **2023**, *651*, 18−26.
(41) Nisar, F.; Malik, M. A.; Mirza, M. A.; Murtaza, G.; Naveed, M. Green synthesis of antimony sulphide (Sb_2S_3) nano-rods in plant oils and study of photocatalytic activity. *Mater. Sci. Eng. B* **2023**, *293*, No. 116467.
(42) Zhao, X.; Gu, M.; Zhai, R.; Zhang, Y.; Jin, M.; Wang, Y.; Li, J.; Cheng, Y.; Xiao, B.; Zhang, J. Violet Antimony Phosphorus with Enhanced Photocatalytic Hydrogen Evolution. *Small* **2023**, *19*, No. e2302859.
(43) Ayappan, C.; Jayaraman, V.; Palanivel, B.; Pandikumar, A.; Mani, A. Facile preparation of novel Sb_2S_3 nanoparticles/rod-like α-Ag_2WO_4 heterojunction photocatalysts: Continuous modulation of band structure towards the efficient removal of organic contaminants. *Sep. Purif. Technol.* **2020**, *236*, No. 116302.
(44) Javaid, A.; Imran, M.; Kanwal, F.; Latif, S.; Adil, S. F.; Shaik, M. R.; Khan, M. Sb-Doped Cerium Molybdate: An Emerging Material as Dielectric and Photocatalyst for the Removal of Diclofenac Potassium from Aqueous Media. *Molecules* **2023**, *28*, 7979.
(45) Javaid, A.; Imran, M.; Kanwal, F.; Latif, S. Antimony-doped cerium ferrite: a robust photocatalyst for the mitigation of diclofenac potassium, an emerging contaminant. *Mater. Sci. Semicon. Proc.* **2024**, *177*, No. 108350.
(46) Feng, Y.; Gong, X.; Fan, S.; Jiang, Z.; Yang, J.; Qu, Y.; Chen, Y.; Peng, Q.; Ding, J.; Shen, H.; Qi, X.; Wang, M. Constructing Robust Interfacial Chemical Bond Enhanced Charge Transfer in S-Scheme 3D/2D Heterojunction for CO_2 Photoreduction. *Adv. Funct. Mater.* **2024**, No. 2403502.
(47) Ackermann, L.; Lin, S. Special Collection on Organic Electrocatalysis. *Eur. J. Org. Chem.* **2023**, *26*, No. e202300214.
(48) Li, Z.; Cheng, Y.; Liu, Y.; Shi, Y. Research progress of two-dimensional antimonene in energy storage and conversion. *Phys. Chem. Chem. Phys.* **2023**, *25*, 12587−12601.
(49) Zhang, S.; Yan, Z.; Li, Y.; Chen, Z.; Zeng, H. Atomically Thin Arsenene and Antimonene: Semimetal−Semiconductor and Indirect−Direct Band-Gap Transitions. *Angew. Chem., Int. Ed. Engl.* **2015**, *54*, 3112−3115.
(50) Wu, X.; Shao, Y.; Liu, H.; Feng, Z.; Wang, Y. L.; Sun, J. T.; Liu, C.; Wang, J. O.; Liu, Z. L.; Zhu, S. Y.; Wang, Y. Q.; Du, S. X.; Shi, Y. G.; Ibrahim, K.; Gao, H. J. Epitaxial Growth and Air-Stability of Monolayer Antimonene on $PdTe_2$. *Adv. Mater.* **2017**, *29*, No. 1605407.
(51) Masibi, K. K.; Fayemi, O. E.; Adekunle, A. S.; Sherif, E. M.; Ebenso, E. E. Electrocatalysis of Lindane Using Antimony Oxide Nanoparticles Based-SWCNT/PANI Nanocomposites. *Front. Chem.* **2018**, *6*, 423.
(52) Fan, G.; Xu, W.; Li, J.; Ni, Y.; Yu, M.; Liu, F.; Cheng, F. Enhancing Electrocatalytic Nitrogen Reduction on Few-Layer Antimonene in an Aqueous Potassium Sulfate Electrolyte. *J. Phys. Chem. C* **2022**, *126*, 13629−13639.
(53) Li, F.; Xue, M.; Li, J.; Ma, X.; Chen, L.; Zhang, X.; MacFarlane, D. R.; Zhang, J. Unlocking the Electrocatalytic Activity of Antimony for CO_2 Reduction by Two-Dimensional Engineering of the Bulk Material. *Angew. Chem., Int. Ed.* **2017**, *56*, 14718−14722.
(54) Ren, X.; Li, Z.; Qiao, H.; Liang, W.; Liu, H.; Zhang, F.; Qi, X.; Liu, Y.; Huang, Z.; Zhang, D.; Li, J.; Zhong, J.; Zhang, H. Few-Layer Antimonene Nanosheet: A Metal-Free Bifunctional Electrocatalyst for Effective Water Splitting. *ACS. Appl. Energy. Mater.* **2019**, *2*, 4774−4781.
(55) Qu, W.; Wang, Z.; Sui, X.; Gu, D. An efficient antimony doped tin oxide and carbon nanotubes hybrid support of Pd catalyst for formic acid electrooxidation. *Int. J. Hydrogen. Energy* **2014**, *39*, 5678−5688.
(56) Deepthi, K. R.; Ramesh, G. V.; Kodiyath, R.; Kumar, P. S. M.; Dakshanamoorthy, A.; Abe, H. Mixed-valence $NaSb_3O_7$ support toward improved electrocatalytic performance in the oxygen-reduction reaction. *J. Mater. Chem. A* **2017**, *5*, 1667−1671.
(57) Christensen, P. A.; Attidekou, P. S.; Egdell, R. G.; Maneelok, S.; Manning, D. A. C.; Palgrave, R. Identification of the Mechanism of Electrocatalytic Ozone Generation on Ni/Sb-SnO_2. *J. Phys. Chem. C* **2017**, *121*, 1188−1199.
(58) Xu, L.; Yi, Y.; Liang, G.; Zhang, W. Antimony doped tin oxide nanoparticles deposited onto Nb-TiO_2 nanotubes for electrochemical degradation of bio-refractory pollutions. *Electroanalysis* **2020**, *32*, 1370−1378.
(59) Deng, D.; Li, Y.; Wu, M.; Song, Y.; Huang, Q.; Duan, Y.; Chang, Y.; Zhao, Y.; He, C. Electrocatalytic Degradation of Rhodamine B on the Sb-Doped SnO_2/Ti Electrode in Alkaline Medium. *ACS. Omega.* **2023**, *8*, 48480−48490.
(60) Liu, Z.; Zhu, M.; Zhao, L.; Deng, C.; Ma, J.; Wang, Z.; Liu, H.; Wang, H. Aqueous tetracycline degradation by coal-based carbon electrocatalytic filtration membrane: Effect of nano antimony-doped tin dioxide coating. *Chem. Eng. J.* **2017**, *314*, 59−68.
(61) Wu, P.; Zhang, A.; Peng, L.; Zhao, F.; Tang, Y.; Zhou, Y.; Yu, G. Cyanogel-Enabled Homogeneous Sb-Ni-C Ternary Framework Electrodes for Enhanced Sodium Storage. *ACS. Nano.* **2018**, *12*, 759−767.
(62) Gunasooriya, G. T. K. K.; Kreider, M. E.; Liu, Y.; Zamora Zeledón, J. A.; Wang, Z.; Valle, E.; Yang, A. C.; Gallo, A.; Sinclair, R.; Stevens, M. B.; Jaramillo, T. F.; Nørskov, J. K. First-Row Transition Metal Antimonates for the Oxygen Reduction Reaction. *ACS. Nano.* **2022**, *16*, 6334−6348.
(63) Kim, D.; Lim, W. G.; Kim, Y.; Oh, L. S.; Kim, S.; Park, J. H.; Jo, C.; Kim, H. J.; Kang, J.; Lee, S.; Lim, E. Amorphous antimony oxide as reaction pathway modulator toward electrocatalytic glycerol oxidation for selective dihydroxyacetone production. *Appl. Catal., B* **2023**, *339*, No. 123104.
(64) Xu, B.; Huang, X.; Liu, S.; Hu, Z.; Kao, C. W.; Chan, T. S.; Geng, H.; Zhang, Y.; Huang, X. Antimony oxides-protected ultrathin Ir-Sb nanowires as bifunctional hydrogen electrocatalysts. *Nano. Res.* **2024**, *17*, 1042−1049.
(65) Zhang, Z.; Fujioka, T.; Koide, T.; Yano, Y.; Ono, T.; Hisaeda, Y. Synthesis of First Antimony Porphycene and Electrocatalytic Hydrogen Evolution Driven by Ligand-Centered Reduction. *B. Chem. Soc. Jpn.* **2021**, *94*, 2048−2053.
(66) Yan, Q. W.; Wu, L. W.; Liu, Z. W.; Chen, F.; Ling, C.; Liu, H. Y.; Xiao, X. Y.; Si, L. P. First application of antimony(III) corrole for

electrocatalytic hydrogen evolution. *Green. Chem.* **2024**, *26*, 4574−4581.
(67) Jiang, J.; Materna, K. L.; Hedström, S.; Yang, K. R.; Crabtree, R. H.; Batista, V. S.; Brudvig, G. W. Antimony Complexes for Electrocatalysis: Activity of a Main-Group Element in Proton Reduction. *Angew. Chem., Int. Ed.* **2017**, *56*, 9111−9115.
(68) Guo, X.; Cao, S. M.; Liu, X.; Huang, C.; Zhou, J. Facile solvothermal preparation of an organic hybrid dysprosium selenidoantimonate for an efficient oxygen evolution reaction. *Dalton. Trans.* **2023**, *52*, 14297−14302.
(69) Ma, S.; Wu, K.; Fan, S.; Li, Y.; Xie, Q.; Ma, J.; Yang, L. Electrocatalytic CO_2 reduction enhanced by Sb doping in MOF-derived carbon-supported Bi-based materials. *Sep. Purif. Technol.* **2024**, *339*, No. 126520.
(70) Olah, G. A. Crossing conventional boundaries in half a century of research. *J. Org. Chem.* **2005**, *70*, 2413−2429.
(71) Pan, B.; Gabbaï, F. P. $[Sb(C_6F_5)_4][B(C_6F_5)_4]$: an air stable, Lewis acidic stibonium salt that activates strong element-fluorine bonds. *J. Am. Chem. Soc.* **2014**, *136*, 9564−9567.
(72) Hirai, M.; Cho, J.; Gabbaï, F. P. Promoting the Hydrosilylation of Benzaldehyde by Using a Dicationic Antimony-Based Lewis Acid: Evidence for the Double Electrophilic Activation of the Carbonyl Substrate. *Chemistry* **2016**, *22*, 6537−6541.
(73) Tofan, D.; Gabbaï, F. P. Fluorinated antimony(V) derivatives: strong Lewis acidic properties and application to the complexation of formaldehyde in aqueous solutions. *Chem. Sci.* **2016**, *7*, 6768−6778.
(74) Smith, J. E.; Gabbaï, F. P. Are Ar_3SbCl_2 Species Lewis Acidic? Exploration of the Concept and Pnictogen Bond Catalysis Using a Geometrically Constrained Example. *Organometallics* **2023**, *42*, 240−245.
(75) Murphy, B. L.; Gabbaï, F. P. Binding, Sensing, And Transporting Anions with Pnictogen Bonds: The Case of Organoantimony Lewis Acids. *J. Am. Chem. Soc.* **2023**, *145*, 19458−19477.
(76) Yang, M.; Pati, N.; Bélanger-Chabot, G.; Hirai, M.; Gabbaï, F. P. Influence of the catalyst structure in the cycloaddition of isocyanates to oxiranes promoted by tetraarylstibonium cations. *Dalton. Trans.* **2018**, *47*, 11843−11850.
(77) Lei, J.; Peng, L.; Qiu, R.; Liu, Y.; Chen, Y.; Au, C. T.; Yin, S. F. Establishing the correlation between catalytic performance and N→Sb donor-acceptor interaction: systematic assessment of azastibocine halide derivatives as water tolerant Lewis acids. *Dalton. Trans.* **2019**, *48*, 8478−8487.
(78) Tang, N.; Song, X.; Yang, T.; Qiu, R.; Yin, S. F. Synthesis and structure of the bimetallic organoantimony catalyst and its application in diastereoselective direct Mannich reaction as facile separation catalytic system. *J. Organomet. Chem.* **2021**, *942*, No. 121820.
(79) Zhang, J.; Wei, J.; Ding, W. Y.; Li, S.; Xiang, S. H.; Tan, B. Asymmetric Pnictogen-Bonding Catalysis: Transfer Hydrogenation by a Chiral Antimony(V) Cation/Anion Pair. *J. Am. Chem. Soc.* **2021**, *143*, 6382−6387.
(80) Pupkova, Y. O.; Sharutin, V. V.; Sharutina, O. K.; Fominykh, A. S.; Eltsov, O. S. Molecular structure and photocatalytic properties of the pentaphenylantimony−3, 5-dinitrosalicylic acid reaction product. *Mendeleev. Commun.* **2022**, *32*, 377−378.
(81) Yan, L.; Liu, Y.; Hu, H.; Li, H.; Shi, L.; Zhang, D. Investigations on the Antimony Promotional Effect on CeO_2−WO_3/TiO_2 for Selective Catalytic Reduction of NO_x with NH_3. *ChemCatChem.* **2016**, *8*, 2267−2278.
(82) Wang, Y.; Lu, J.; Ma, X.; Niu, Y.; Singh, V.; Ma, P.; Zhang, C.; Niu, J.; Wang, J. Synthesis, characterization and catalytic oxidation of organosilanes with a novel multilayer polyoxomolybdate containing mixed-valence antimony. *Mol. Catal.* **2018**, *452*, 167−174.
(83) Alshehri, A.; Narasimharao, K. Antimony Substituted Ammonium 12-Molybdophosphoric Acid Catalysts for Gas Phase Chlorobenzene Oxidation. *Catal. Lett.* **2021**, *151*, 1025−1037.
(84) Lu, J.; Bu, Z.; Lei, Y.; Wang, D.; He, B.; Wang, J.; Huang, W. Facile microwave-assisted synthesis of Sb_2O_3-CuO nanocomposites for catalytic degradation of p-nitrophenol. *J. Mol. Liq.* **2024**, *409*, No. 125503.
(85) Chitnis, S. S.; Sparkes, H. A.; Annibale, V. T.; Pridmore, N. E.; Oliver, A. M.; Manners, I. Addition of a Cyclophosphine to Nitriles: An Inorganic Click Reaction Featuring Protio, Organo, and Main-Group Catalysis. *Angew. Chem., Int. Ed. Engl.* **2017**, *56*, 9536−9540.
(86) Gini, A.; Paraja, M.; Galmés, B.; Besnard, C.; Poblador-Bahamonde, A. I.; Sakai, N.; Frontera, A.; Matile, S. Pnictogen-bonding catalysis: brevetoxin-type polyether cyclizations. *Chem. Sci.* **2020**, *11*, 7086−7091.
(87) Simion, A.; Candu, N.; Cojocaru, B.; Coman, S.; Bucur, C.; Forneli, A.; Primo, A.; Man, I. C.; Parvulescu, V. I.; Garcia, H. Nanometer-thick films of antimony oxide nanoparticles grafted on defective graphenes as heterogeneous base catalysts for coupling reactions. *J. Catal.* **2020**, *390*, 135−149.

https://doi.org/10.1021/acsorginorgau.4c00072
ACS Org. Inorg. Au 2025, 5, 13−25